AD-A160 902 THREE-DIMENSIONAL TRANSONIC ROTOR FLOW FIELD RECONSTRUCTED FROM HOLOGRAPH..(U) NATIONAL AERONUATICS AND SPACE ADMINISTRATION MOFFETT FIELD C.. 1/1

UNCLASSIFIED J K KITTLESON ET AL. OCT 85 NASA-A85347 F/G 20/4 NL

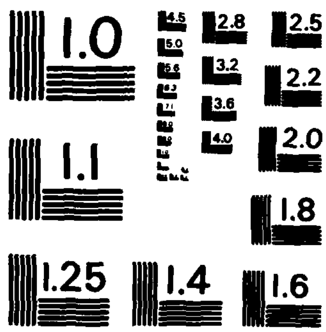

MICROCOPY RESOLUTION TEST CHART
NATIONAL BUREAU OF STANDARDS-1963-A

(2)

NASA Technical Memorandum 86816 USAAVSCOM Technical Report 85-A 10

AD-A160 902

Three-Dimensional, Transonic Rotor Flow Field Reconstructed from Holographic Interferogram Data

John K. Kittleson, Yung H. Yu, and Friedhelm Becker

October 1985

NASA
National Aeronautics and
Space Administration

United States Army
Aviation Systems
Command

NASA Technical Memorandum 86816 USAAVSCOM Technical Report 85-A-10

Three-Dimensional, Transonic Rotor Flow Field Reconstructed from Holographic Interferogram Data

John K. Kittleson,
Yung H. Yu, Aeroflightdynamics Directorate, U. S. Army Aviation Research and Technology Activity-AVSCOM
Ames Research Center, Moffett Field, California
Friedhelm Becker, Max-Planck-Institut fuer Stroemungsforschung
Goettingen, West Germany

Accession For		
NTIS GRA&I		X
DTIC TAB		☐
Unannounced		☐
Justification		
By		
Distribution/		
Availability Codes		
Dist	Avail and/or Special	
A-1		

QUALITY INSPECTED 5

October 1985

National Aeronautics and Space Administration

Ames Research Center
Moffett Field, California 94035

United States Army
Aviation Systems
Command
St. Louis, Missouri 63120

THREE-DIMENSIONAL, TRANSONIC ROTOR FLOW FIELD RECONSTRUCTED FROM HOLOGRAPHIC INTERFEROGRAM DATA

John K. Kittleson and Yung H. Yu
Research Scientists
Aeroflightdynamics Directorate, U. S. Army Aviation Research and Technology Activity -- AVSCOM
Ames Research Center, Moffett Field, California

and

Friedhelm Becker
Research Scientist
Max-Planck-Institut fuer Stroemungsforschung
Goettingen, West Germany

Summary

Holographic interferometry and computer-assisted tomography (CAT) are used to determine the transonic flow field of a model rotor blade in hover. A pulsed ruby laser recorded 40 interferograms with a 61 cm-diam view field near the model rotor-blade tip operating at a tip Mach number of 0.90. After digitizing the interferograms and extracting fringe-order functions, the data are transferred to a CAT code. The CAT code then calculates pressure coefficients in several planes above the blade surface. The values from the holography-CAT method compare favorably with previously obtained numerical computations and laser velocimeter measurements at most locations near the blade tip. The results demonstrate the technique's potential for three-dimensional transonic rotor flow studies.

1. INTRODUCTION

On many helicopters, the rotor blade's advancing tip encounters transonic flow during forward flight. At these high Mach numbers, the rotor blade's performance suffers from compressibility effects that often cause shock waves to form near the blade tip; the shocks can extend to the acoustic far-field [1]. Through theoretical and computational investigations, researchers attempt to understand the local shock generation of high-tip-speed rotors and its propagation to the far-field. However, because of the problem's complexity and the difficulty of obtaining detailed experimental information about the flow, accurate means for confirming transonic rotor-blade designs have been notably lacking.

In an attempt to describe the transonic rotor flow field and to resolve the problems associated with it, promising theoretical models [2] and numerical codes [3,4] have been developed. The numerical codes compare favorably with blade-pressure measurements [5], but are not yet verified at points away from the blade's surface.

Holographic interferometry is an effective diagnostic technique for making transonic flow measurements [6]. Previous investigations [7,8] in which two-dimensional flows over airfoils were studied show that accurate quantitative information is obtainable using holographic interferometry. However, the transonic flow around a helicopter rotor blade is three-dimensional and requires a tomographic technique to compute the correct flow information from several interferograms. To date, most applications of this technique have been limited to axisymmetric flow or to simple three-dimensional flow with a small model under ideal laboratory conditions [9,10].

This paper discusses the procedures necessary to obtain quantitative measurements of a transonic, three-dimensional flow field near a rotor-blade tip, using holographic interferometric data and computer-assisted tomography (CAT). Though most helicopter rotor problems caused by shock waves occur during forward flight, this experiment investigates the steady problem (hover), which simulates many physical phenomena of forward flight [11]. The method for recording interferograms and example interferograms is included, and the steps required for extracting quantitative information from the interferograms are outlined. The technique's potential for measuring three-dimensional transonic rotor flows is demonstrated, and the results of using this technique are compared with those from previously performed numerical computations and laser velocimeter measurements.

2. BACKGROUND CONCEPTS

For the experiment to be successful, it is necessary to 1) record high-quality interferograms near a rotor-blade tip from multiple viewing angles, and 2) implement a suitable CAT code with the interferogram data. Familiarity with holography, holographic interferometry, and computer-assisted tomography principles provides the necessary insight for understanding this technique.

2.1 Holography

Holography is a two-step imaging process in which diffracted light waves are recorded and reconstructed [12,13]. The first step is recording, or storing, the hologram. This is accomplished by dividing a single coherent laser beam into two beams and exposing a photographic film to the two light waves. The object wave, which is the wave containing the flow information, passes through the measured field (the air near the blade tip in this experiment). The second wave, the reference wave, passes around the field. By adding the coherent reference wave to the object wave, the photographic film records a high-frequency interference pattern. Once the film is developed, it is known as a hologram, which is a complicated diffraction grating.

The second step in holography is reconstruction, or playing back the hologram. This is accomplished in two ways. First, a reconstruction wave identical to the reference wave illuminates the hologram. The hologram diffracts the reconstruction wave and produces a replica of the original object wave, forming the original object's virtual image. In the second method of reconstruction, a reconstruction wave which is conjugate to the reference wave, illuminates the hologram. The hologram diffracts the conjugate wave forming the original object's real image. The real image may be photographed without the use of a lens by placing a sheet of photographic film in the real image space.

Several important characteristics of holography are applicable to the experiment at hand. There are very few geometrical constraints in a holographic optical system; thus, holography can be applied in a large-scale, nonlaboratory environment. Note that recording and reconstruction of the hologram can be done in different locations if the reference wave is reproducible. This allows the reconstruction to be done in a laboratory, far from the harsh environment in which the hologram was previously recorded. The reference wave serves only as a method of recording and reconstructing the object wave. Thus, a hologram does not produce quantitative information about the field of interest. To obtain quantitative information (in the form of interference fringes) an interferogram must be recorded.

2.2 Holographic Interferometry

Holographic interferometry is the interferometric comparison of two object waves recorded holographically (see ref. 12 for further detail). In this experiment, the two object waves are recorded sequentially in time with double-exposure holographic interferometry. The interferogram is recorded by first exposing a photographic file to a first reference wave and an "undisturbed" object wave. Later in time, the same photographic film is exposed to a second reference wave and to a second "disturbed" object wave.

When the holographic interferogram is reconstructed, the virtual or real image shows the object (the transparent field) with an interference fringe pattern. The fringe pattern represents the difference between the "undisturbed" and "disturbed" flow states. The irradiance of the reconstructed wave is proportional to

$$I = |U_{o1} + U_{o2}|^2$$

where U_{o1} and U_{o2} are the complex amplitude of the first and second object waves, which can also be written

$$I = 2A^2[I + \cos(\Delta\phi)] \quad (1)$$

Equation (1) represents the interferogram with a fringe pattern of dark and bright fringes of constant optical path-length difference (OPD) $\Delta\phi$. $\Delta\phi$ is given by

$$\Delta\phi = \int [n(x,y,z) - n_0] ds = N\lambda \quad (2)$$

where n is the refractive index, N is the fringe-order number, and λ is the laser wavelength. To determine the flow-field properties, the line integral of Eq. (2) must be inverted and solved for $n(x,y,z)$, the refractive index at a specific point in the field.

In a two-dimensional flow (i.e., the flow over a fixed airfoil in a wind tunnel), the evaluation of Eq. (2) is simplified. Since the refractive index is assumed constant along the probing rays, equation [2] becomes

$$n(x) = n_0 + N\lambda/L \quad (3)$$

in a horizontal plane (y = const) at any location z across the test section of width L. In a two-dimensional flow, the fringes on an interferogram are contours of constant refractive index, thus the refractive index at any point in the field can be determined from a single interferogram. In

the general asymmetric case (i.e., the flow field near a rotor-blade tip), however, equation [3] cannot be used. A set of interferograms must be recorded at different viewing angles around the field in order to reconstruct the flow field. The refractive index at any given point in the flow field may then be obtained by applying the methods of computer-assisted tomography to invert the integral equation [2].

2.3 Computer-Assisted Tomography

Tomography is a mathematical technique for reconstructing a three-dimensional field from its two-dimensional projections (see refs. 14 and 15 for a wide variety of applications). A projection of a three-dimensional field is the fringe pattern recorded on an interferogram. All methods require multidirectional projection data of the field. Tomographic codes develop in two directions: 1) iterative algebraic reconstruction techniques [16], and 2) Fourier transform techniques. A version of the latter method, termed filtered back-projection [17,18] appears most suitable for this application.

Most Fourier transform techniques employ back-projection. Projection data from the field are recorded in one plane at several azimuthal angles around the field. For example, one projection of a uniform absorbing disk is shown in figure 1a (taken from ref. 19). Beyond the disk boundary (no path length through the disk), the light ray's OPD is unchanged, producing no interference fringes. Near the disk boundary (short path length through the disk), the light ray's OPD is changed slightly, producing a few interference fringes. And near the disk center (long path length through the absorbing disk), the light ray's OPD is changed substantially, producing several interference fringes. Similar projections (fringe number vs. position) at different azimuthal angles are also recorded. Each projection is then back-projected, or smeared back along the direction in which it was recorded (fig. 1b). Values are added, point by point, to form a reconstruction of the field. Unfortunately, simple back-projection produces an undesirable spoke pattern which severely degrades the quality of the reconstructed field.

To eliminate the spoke pattern, the back-projections are filtered. A one-dimensional convolution (indicated by an asterisk in the following equation) is performed between each projection and an appropriate filter function (see ref. 20 for a discussion of filter functions) before back-projection, as shown in fig. 2a (taken from ref. 19). Each filtered projection is then back-projected over the reconstruction space (see fig. 2b). The negative side-lobes introduced by the filter eliminate the spoke pattern during the point-by-point addition process. The convoluted back-projection is given as

$$n(x,z) = \int_0^{\pi} \int_{-\infty}^{\infty} N_\theta(\xi) * F^{-1}(|f|)\delta(x \sin\theta + z\cos\theta - \xi)\,d\xi\,d\theta$$

where $n(x,z)$ is the reconstructed field function (refractive index) in a horizontal plane (y = const), and $N_\theta(\xi)$ are the cross sections through the fringe-order function at angle ξ to be convolved with the inverse Fourier transform of the abs-function. The integration of the convolved "projection" is done along lines expressed as

$$\delta(x \sin\theta + z\cos\theta - \xi)$$

and overall projections θ. With many projections, this technique yields an accurate reconstruction of the original field in one plane. This procedure is repeated using data in several planes to yield a reconstruction of the entire three-dimensional field.

3. PROCEDURE

Several steps must be performed to quantitatively reconstruct the three-dimensional transonic field near a model helicopter blade tip. First, several holographic interferograms must be recorded along lines perpendicular to the rotor tip-path plane at various azimuthal angles (fig. 3). Data must then be extracted from the interferograms. This can be done 1) by hand, 2) by using a graphic tracing tablet [21], or 3) by using a system that digitizes the interferograms and extracts fringe-order numbers. The digital interferogram evaluation technique was used, and is presented in detail by Becker and Yu [22]. Finally, the data are transferred as input to a tomography code, which computes the refractive index at specific points in a horizontal plane above the blade surface. This procedure is repeated in several planes to yield a reconstruction of the entire three-dimensional field.

3.1 Holographic Interferogram Recording

The holographic system for recording interferograms near a model rotor blade was assembled in the Aeroflightdynamics Directorate Anechoic Hover Chamber. Figure 4 shows a schematic of the optical system and fig. 5 shows the Anechoic Hover Chamber. A ruby laser with a 20-nsec pulse width, a 694.3-nm wavelength, and a power of 1 J "freezes" the rotating blade at any desired azimuthal angle. A beam-splitter divides the laser beam into two separate beams at the laser outlet. A microscope objective lens expands the object

beam to fill a 61 cm-diam spherical mirror. Since the foci of both the objective lens and the spherical mirror coincide, a collimated plane wave forms as the beam passes through the rotor area. The object beam then strikes a second 61 cm-diam spherical mirror, emerges as a converging wave, and illuminates a 10.2 cm by 12.7 cm photographic plate. The reference beam is lengthened by causing it to strike several plane mirrors. This beam must be lengthened so that the difference in the path lengths of the object and reference beams is less than the coherence length of the laser (one of the very few, and easily met, geometrical constraints in a holographic system). The reference beam is expanded by an objective lens, then collimated with a 12.7 cm-diam lens; finally, it is directed toward the film so that it overlaps the object beam.

The entire procedure is conducted from outside the hover chamber, once the optical system is aligned. Firing the laser, changing the photographic film plates, and controlling the test conditions are all done by remote control. Recall that to record an interferogram, two exposures at different times (different flow states) must be made on a single film plate. The film records the first exposure while the rotor blade remains stationary. In this case, the air has no velocity and therefore has a uniform refractive-index distribution. The film records the second exposure while the blade rotates at the desired speed. The nonhomogeneous refractive-index distribution in this case introduces phase changes in the second object wave, producing interference fringes on the film plate. This double-exposure recording procedure repeats at various angles around the flow by synchronizing the laser pulse with the desired blade position. Because of the long optical pathlengths (27 m), the recording system is very sensitive to vibrations of the optical components. At several azimuthal angles, it was necessary to record multiple interferograms to obtain one high-quality interferogram. The photographic plates are then removed from the recording system in the hover chamber, developed, and reconstructed in a laboratory for further processing.

Holographic interferograms record the flow near a hovering 1/7-scale (geometric) model UH-1H rotor with untwisted NACA 0012 airfoil sections. The blade runs at a tip Mach number of 0.90 so that the flow is transonic and a shock wave is present [1]. This model normally uses two blades; however, in views along the span, the optical beam would pass through the refractive-index field of both blades. Because the refractive-index fields of the two blades are inseparable at these angles, a single-bladed rotor with a counterbalance is used instead (fig. 6).

Holographic interferograms near a transonic rotor blade are sequentially recorded at 40 different viewing angles. Figure 7 shows a simplified schematic plan view of the optical system near the blade area. The blade rotates in a clockwise direction and is captured at any desired viewing angle with the pulsed laser. The optical system translates laterally to insure that the laser beam passes near the blade-tip area. The tomography code requires flow data from certain viewing angles within a 180° range. Numerical simulation results [23] using numerical computations of the flow [3] suggest recording interferograms from $\theta = 8°$ to $\theta = 40°$, and from $\theta = 140°$ to $\theta = 186°$ in 2° increments, as defined in fig. 7. The missing views, $\theta = 42°$ to $\theta = 138°$, were presumed to have very few interference fringes and were not utilized.

Illustrated in fig. 7 are examples of holographic interferograms recorded near the model blade tip. The fringe pattern's appearance depends on the viewing direction. Interferograms recorded along the chord (near $\theta = 90°$) display very few interference fringes, since the optical rays pass through the field's thinnest (weakest) region. No observable details are present in these views. However, in views along the span (near $\theta = 0°$ or $\theta = 180°$), numerous fringes are visible, because the optical rays pass through the longest (strongest) region within the field. The leading-edge stagnation point, shock structures, boundary-layer separation, and wake system are clearly visible. In particular, a lambda shock ($\theta = 180°$) and the radiated shock ($\theta = 186°$) appear above the blade. Several interferograms are described in detail in reference 24.

3.2 Data Extraction

One important step between recording the interferograms and applying tomographic reconstruction techniques is the evaluation of the interferograms; that is, reading fringe positions and fringe numbers. Up to now, most interferograms from aerodynamic tests have been evaluated by either reading fringe numbers and their positions manually or by tracing the fringe lines by hand with the help of a tracking device (for instance a graphic tablet). However, manual evaluation is a very time-consuming and inaccurate procedure. Also, it is evident that in the current application, where large numbers of interferograms have to be evaluated at several horizontal planes, utilization of an automatic fringe-reading procedure would enhance the evaluation and would make the interferometric technique a much more powerful measurement tool. (See reference 22 for a detailed discussion of this procedure.)

To reconstruct the three-dimensional flow field from these interferograms, using tomographic reconstruction techniques, requires the fringe number-functions along cross sections of a plane parallel to the rotor disk. Data from all the views are needed to reconstruct the refractive

index in a particular plane above the blade. Several planes have to be reconstructed to get a three-dimensional flow-field representation. This procedure requires that each interferogram be represented in a form that allows the fringe-order function to be computed at any desired point.

The evaluation of interferograms using computer-aided methods can be subdivided into the following steps: 1) interferogram digitizing and image enhancing, 2) fringe segmenting and fringe-coordinate extracting, 3) obtaining fringe fields from several magnified views and merging, 4) fringe numbering and correcting fringe disconnections, 5) transforming coordinates, 6) interpolating and extrapolating fringe-number functions. In the following, a system is briefly described for evaluating interferograms that incorporates the evaluation steps mentioned above.

3.2.1 Hardware Components. An image-processing system (De Anza IP-6400) connected to a VAX 11/780 host computer provides the main hardware necessary for digitizing the interferograms and for doing some image-enhancement processing. The resolution of the system is 512 × 512 pixels with an 8-bit intensity range. Currently it is equipped with two of possible four memory planes, as well as with a graphic and an alphanumeric overlay. A frame-grabbing unit can digitize a frame of a video signal in real time (1/30 sec). A black and white video camera (MTI series 68) with a resolution (bandwidth) of 18 MHz is connected to this input channel.

The system has an arithmetic-logic unit (ALU), with which real-time addition, subtraction, or comparison of one or more image planes may be made. The contents of each memory plane may be routed through lookup tables before being input to the ALU, to the video-output processor, or to another plane. The actual contents of any image plane, or of a combination of image planes, is output via a video-output processor and can be shown on a color-display. Each channel has its own color-mapping tables. A joystick control device is used for interactive input. It controls two cursors, which may be used in a number of different operating modes. A color print system (Dunn Instruments model 631) serves as a hardcopy device for the color monitor.

3.2.2 Digitization and Processing. During the recording of the holographic interferograms, two fiducial points were marked in the image plane with a known position relative to the rotor system. This allowed a subsequent coordinate transformation into a space-fixed coordinate system. Each interferogram was then digitized, and several subsections were enlarged, depending on the fringe density in the interferograms. A scale, aligned to the fiducial marks, was always digitized together with the interferogram so that the position and magnification of the enlarged segments could be identified. Before segmentation and fringe-coordinate extraction are applied, it may be useful to do some image enhancement to reduce noise. Frame-averaging methods increase the signal-to-noise ratio of the imaging electronic components, thereby improving the picture quality.

3.2.3 One-Dimensional Evaluation. One-dimensional interactive processing may be employed, if only one two-dimensional plane of the flow field is reconstructed; hence, only one cross section through each interferogram has to be known. In this case some of the expense required for the full two-dimensional evaluation of the fringe pattern may be avoided. But the procedure has to be interactive, because local information (i.e., knowledge of the fringe locations along one line) is not sufficient to number the fringes correctly or to detect lost fringes or other distortions. In an interactive procedure, information such as acceptance of the segmentation and assignment of fringe numbers has to be given by the user.

A program featuring the one-dimensional evaluation digitizes and preprocesses an interferogram and does a fringe segmentation along a line, or along a set of lines, through the field of view. The result of the segmentation procedure (a binary fringe pattern) is written back to the image screen for monitoring reasons (see figs. 8a and 8b). Users may interactively change the acceptance threshold or edit the segmented cross section in heavily distorted regions before they continue to the numbering section. The cursor can be moved to each part of the segmented line, and fringe numbers may be assigned interactively by various commands. The task assigning fringe numbers is supported by color coding the black parts of the fringes; this shows whether the fringe-order function increases or decreases by 1, or if a discontinuity is present between adjacent fringes. The resulting fringe-order function may also be plotted onto a graphic terminal. A post-processing program merges all the data taken from different enlarged portions of an interferogram (as shown in figs. 8a and 8b) and uses a spline-approximation to interpolate between the fringes. The final result is extracting the fringe order function at a desired height above the blade surface as shown in figure 8c.

3.2.4 Two-Dimensional Interactive Processing. Often the knowledge of only a cross section across the field of view is not sufficient for interpreting a given flow problem; instead, the fringe patterns have to be evaluated over the whole field of view. To facilitate the two-dimensional interferogram evaluation, additional algorithms have been implemented to segment fringes, to extract

each fringe's coordinates (trace the fringe sides), and to represent the whole fringe field as a polygonal data structure. Methods for numbering these line fields and detecting extracting errors have been developed. With a two-dimensional interpolation scheme, fractional fringe-order numbers may then be estimated at any given point in the field of view.

Figure 9 shows an example of a typical fringe-coordinate extraction. An interferogram (fig. 9a) is digitized over the whole field of view with low resolution. The white lines overlaying the display represent the extracted fringe sides, and the black line represents the border polygon. The border polygon was input by hand before the coordinate extraction in order to mask off background objects and the part of the fringe field with high fringe density. (In our implementation, all the graphics are in color and therefore easier to distinguish from the displayed image.)

As was discussed before, it may be necessary to digitize enlarged subsections to resolve regions with high fringe densities. The resulting fringe polygonal field is then combined out of all the individual digitized and processed subsections, starting with the one with highest resolution. To handle the problem of partly overlapping polygonal line fields, a boundary polygon is maintained for each subsection. This defines the definition area for each fringe polygonal field. Upon combination of two overlapping fields, the border polygon of the one with higher resolution (priority) is used to intersect the lines of the other field. Both line fields are then connected at those intersection points. The new border polygon is the border of the combined areas. Figure 9b shows an enlarged digitized part of the interferogram shown in fig. 9a, with the extracted fringe polygons overlaying.

3.3 CAT Reconstruction

Fringe-order functions are transferred to the filtered back-projection CAT code which computes the refractive-index field at specific points in a chosen horizontal plane above the blade surface. The code assumes refractionless light rays; therefore, each horizontal plane can be treated independently, even though data for each plane is taken from one set of interferograms. The pressure coefficient is computed by first converting refractive index to density, using the Gladston-Dale relation:

$$\rho/\rho_0 = (n - 1)/(n_0 - 1)$$

Density is then converted to pressure coefficient from a form of Bernoulli's equation for steady (with respect to the rotation blade), compressible, isentropic flow. The procedure is repeated in several planes above the blade to reconstruct the entire three-dimensional field near the model blade tip.

4. RECONSTRUCTION RESULTS

The holography-CAT reconstruction of the blade-tip pressure coefficient (C_p) field is compared with numerical computations and laser velocimeter (LDV) measurements. The computations used here are conservative, mixed-difference solutions of the transonic small-disturbance equation [3]. The LDV measurements obtained by Owens et al. [25] were recorded using the same test facility and blades as the holographic experiment. All results were obtained with a tip Mach number of 0.90. Results from these three sources are presented in three horizontal planes above the airfoil center axis. Three plot types are used to visualize the flow field. First, C_p contours are displayed comparing the holography-CAT reconstruction and the numerical computations. The contours are given in plan view, where the blade's leading and trailing edges are $X/C = 0.0$ and $X/C = 1.0$, respectively. The blade tip is located at $R/R_0 = 1.0$, the rotation center is at $R/R_0 = 0.0$, and the blade rotates in a clockwise direction. Second, perspective views are displayed in which negative C_p values are plotted along the vertical axis. The data and geometry are identical to the contour plots, though the data are viewed from near the rotor hub. Third, C_p distributions from all three sources are shown at several radial locations.

Figure 10 compares C_p contours derived from the holographic-CAT method and the numerical computations near the blade surface ($Y/C = 0.08$). Both results display high-C_p regions near the leading and trailing edges. They also display a low-C_p region over the blade surface, containing a shock at approximately $X/C = 0.60$ near the blade tip. The general contour shapes show strong resemblance except near the blade tip (roughly the last 5% of blade span). The minimum C_p region appears at the shock foot in the computational analysis, but it appears closer to the leading edge and farther from the shock foot in the holography-CAT results.

Figure 11 shows C_p values for the same plane in perspective view. Again, the general flow shapes appear very similar. The major difference here between the two results is the roughness (minor "ridges") in the reconstructed flow. This may be due to reconstruction artifacts caused by noncontinuous data (interferograms recorded in 2 azimuthal increments) or, more likely, by noise (erroneous fringes) in the interferogram data caused by optical component motion. Figure 12 compares C_p distributions from the holographic-CAT reconstruction, numerical computations, and LDV

measurements (where available). The roughness of the reconstructed flow can be seen throughout the figures. Also, the holography-CAT method determines the shock location to be slightly aft (3-5%) of the numerical results or LDV measurements (see fig. 12c). The major differences can be observed in fig. 12d, where the discrepancies at the leading edge and over the blade surface are clearly visible. Note that all three methods give different results, especially over the blade surface.

Figure 13 compares C_p contours from both the holography-CAT method and the numerical computations at $Y/C = 0.22$ above the blade center axis. The general C_p contours show an excellent agreement in both shape and magnitude throughout this plane. The minimum C_p region above the blade (near $X/C = 0.50$, $R/R_o = 0.96$) matches much closer in this plane than in the plane near the blade surface (fig. 10). The perspective view of fig. 14 also shows an excellent agreement in shape and magnitude. Again, the most noticeable difference in the reconstructed flow is the extra ridges at the same locations and orientations as seen in the previous plane (fig. 11a). The holography-CAT C_p distributions in this plane (fig. 15) compare favorably, especially inboard the blade tip (see figs. 15a-15c). Even at the blade tip (fig. 15d), the holography-CAT reconstruction shape and magnitude agree more closely with the other methods than in fig. 12d.

Finally, fig. 16 compares C_p contours from the holography-CAT method and numerical computations for $Y/C = 0.49$ above the blade. The C_p contour shapes and magnitudes are similar in all regions, except that the holography-CAT results show the minimum C_p point to be slightly (1% span) outboard of the numerical result. The extra ridges seen in perspective view (fig. 17a) are in approximately the same location and orientation as in previous planes; however, the magnitude of the ridges has decreased. Figure 18 shows C_p distributions for $Y/C = 0.49$. There is good agreement at all locations. The most noticeable differences are the shock location in fig. 18a (holography-CAT results slightly aft) and the magnitude in fig. 18d (holography-CAT results slightly larger).

Overall, the comparison of the holography-CAT reconstruction with numerical computations and LDV measurements is extremely encouraging in most regions of the flow field. However, comparisons with other numerical code computations and other experimental data (i.e., hot wire measurements) are required before a final evaluation can be made about the holography-CAT results. Several discrepancies must be resolved. First, the shock location must be confirmed (perhaps through pressure-instrumented blade measurements). Second, the extra ridges appearing in the reconstructed results must be reduced or eliminated. The ridges are most likely caused by poor data recorded in the interferograms. To improve the interferograms' quality, a modified optical system (for both hover and forward flight testing) is necessary. In addition, all methods were unable to predict the expected shock strength beyond the blade tip. Acoustic measurements indicate a much stronger radiated shock than is indicated by these three results.

5. CONCLUDING REMARKS

The holographic interferometry computer-assisted tomography technique proved to be a highly-effective way of measuring the three-dimensional, transonic flow field near a model rotor-blade tip. Results from this method compare favorably with those of numerical computations and laser velocimeter measurement except very near the tip region. In other regions, the C_p distributions along the chord are similar in both shape and magnitude. However, the results from the technique must be further verified against other experimental data.

Since this is the first successful implementation of the holographic interferometry, computer-assisted tomography method in rotor flow studies, many improvements are indicated. For example, the optical system must be improved so that better quality interferograms can be recorded, and an automatic fringe-reading technique must be completed so that the time required to evaluate interferograms can be shortened. Upon verification of these results and after the system is improved, measurements of other model rotor-blade flow fields, including those of forward flight, will be performed.

6. ACKNOWLEDGMENTS

We gratefully acknowledge the support and contributions of several colleagues at the Aeroflightdynamics Directorate: Dr. Fredric H. Schmitz for his inspiration and untiring support; and Dr. Frank X. Caradonna for providing the transonic numerical data shown in this paper. We thank Professor L. Hesselink of Stanford University for performing the numerical simulations, and Professor Charles M. Vest of the University of Michigan for many fruitful discussions and guidance.

REFERENCES

[1] Schmitz, F. H. and Yu, Y. H., "Transonic Rotor Noise--Theoretical and Experimental Comparisons," Vertica, Vol. 5, 1981, pp. 55-74.

[2] Isom, M. P., "Unsteady Subsonic and Transonic Potential Flow Over Helicopter Rotor Blades," NASA CR-2463, 1974.

[3] Caradonna, F. X., "The Transonic Flow on a Helicopter Rotor," Ph.D. dissertation, Stanford U., Stanford, Calif., Mar. 1978.

[4] Arieli, R. and Tauber, M., "Computation of Subsonic and Transonic Flow about Lifting Rotor Blades," AIAA Paper 79-1667, 1979.

[5] Tung, C., Caradonna, F. X., and Boxwell, D. A., "The Prediction of Transonic Flows on Advancing Rotors," Proceedings of the 40th Annual National Forum of the American Helicopter Society, Arlington, Va., May 1984.

[6] Trolinger, J. D., Laser Instrumentation for Flow Field Diagnostics," AGARDograph 186, 1974.

[7] Johnson, D. A. and Bachalo, W. D., "Transonic Flow About a Two-Dimensional Airfoil--Inviscid and Turbulent Flow Properties," AIAA Paper 78-1117, 1978.

[8] Bachalo, W. D., "Measurements of Supercritical Airfoil Flow Fields Using Interferometry," Douglas Aircraft Company, McDonnell Douglas Corporation, Mar. 1982.

[9] Matulka, R. D. and Collins, D. J., "Determination of Three-Dimensional Density Fields from Holographic Interferometry," Journal of Applied Physics, Vol. 42, 197', pp. 1109-1119.

[10] Sweeney, D. W. and Vest, C. M., "Reconstruction of Three-Dimensional Refractive Index Fields from Multidirectional Interferometric Data," Applied Optics, Vol. 12, 1973, pp. 2649-2664.

[11] Boxwell, D. A., Yu, Y. H., and Schmitz, F. H., "Hovering Impulsive Noise: Some Measured and Calculated Results," Vertica, Vol. 3, 1979, pp. 35-45.

[12] Vest, C. M., Holographic Interferometry, Wiley-Interscience, 1979.

[13] Collier, R. J., Burckhardt, C. B., and Lin, L. H., Optical Holography, Academic Press, 1971.

[14] Marr, E. B., ed., Proceedings of the International Workshop on Techniques of Three-Dimensional Reconstruction, BNL 20425, Brookhaven National Laboratory, Upton, N.Y., 1976.

[15] Technical Digest of the 1975 Optical Society of American Technical Meeting, Stanford University, OSA, Washington, D.C., 1975.

[16] Gordon, R. and Herman, G. T., International Review of Cytology, Vol. 38, 1974.

[17] Shepp, L. A. and Logan, B. F., "The Fourier Reconstruction of a Head Section," IEEE Transactions on Nuclear Science, Vol. NS-21, 1974, pp. 21-42.

[18] Ramachandran, G. N. and Lakshminarayanan, A. V., "Three-Dimensional Reconstruction from Radiographic and Electron Micrographic Applications of Convolutions Instead of Fourier Transforms," Proceedings of the National Academy of Sciences of the United States of America, Vol. 68, 1971, pp. 2236-2240.

[19] Swindell, W. and Barrett, H. H., "Computerized Tomography: Taking Sectional X-rays," Physics Today, Dec. 1977, pp. 32-41.

[20] Herman, G. T., "Image Reconstruction from Projections, Implementation and Applications," Topics in Applied Physics, Vol. 32, Springer, Berlin, 1979.

[21] Modarress, D., Tan, H., and Trolinger, J., "Tomographic Reconstruction of Three-Dimensional Flow over Airfoils," Paper No. 85-0479 presented at AIAA 23rd Aerospace Sciences Conference, Reno, Nev., Jan. 14-17, 1985.

[22] Becker, F. and Yu, Y. H., "Application of Digital Interferogram Evaluation Technique to the Measurement of Three-Dimensional Flow Fields," Paper No. 85-0037 presented at AIAA 23rd Aerospace Sciences Conference, Reno, Nev., Jan. 14-17, 1985.

[23] Snyder, R. and Hesselink, L., "Optical Tomography for Flow Visualization of the Density Field Around a Revolving Helicopter Rotor Blade," Applied Optics, Vol. 23, 1984, pp. 3650-3656.

[24] Kittleson, J. K., "A Holographic Interferometry Technique for Measuring Transonic Flow near a Rotor Blade," Proceedings of the Ninth European Rotorcraft Forum, 8, Stresa, Italy, Sept 1983.

[25] Owen, F. K., Orngard, G. M., and McDevitt, T. K., "Laser Velocimeter Measurements of Model Helicopter Rotor Flow Fields," NASA CR-11080, July 1984.

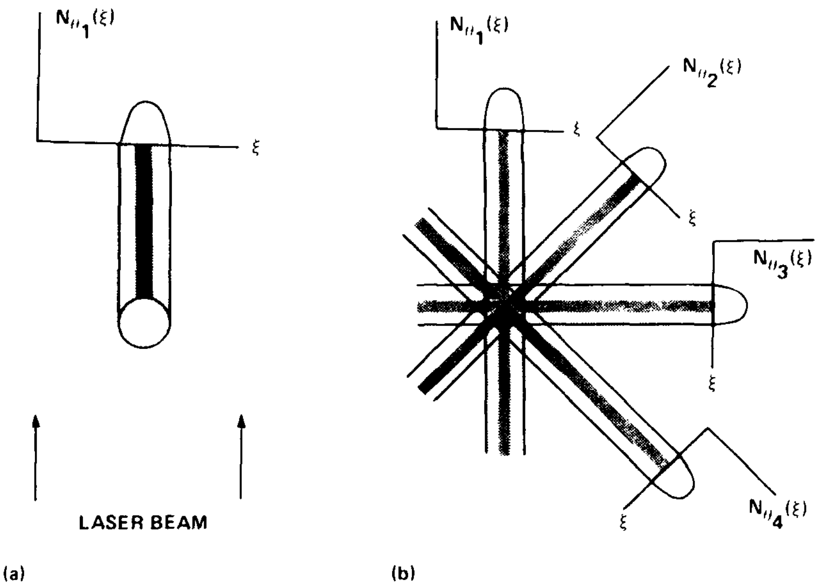

Fig. 1 Back-projection. a) One projection of an absorbing disk; b) back-projecting consists of smearing each projection back along the direction in which the original projection was made (from ref. 19).

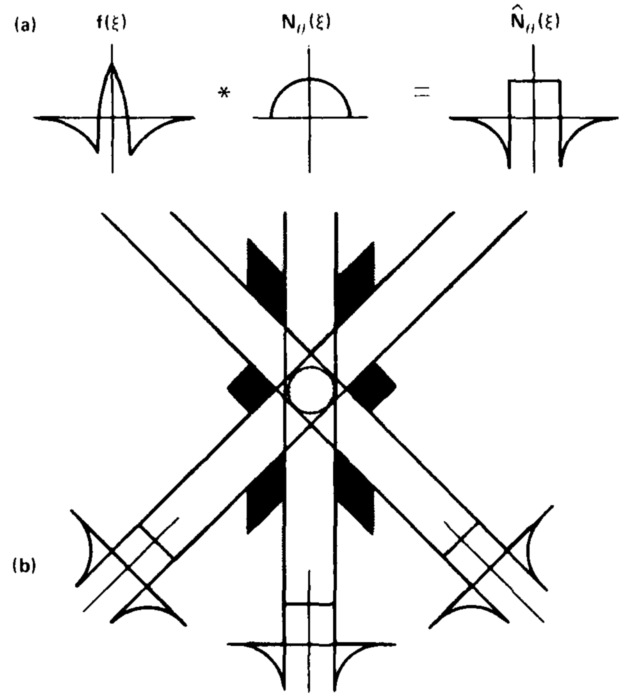

Fig. 2 Filtered back projection. a) The projection data are convolved (filtered) with a suitable processing function before back-projection; b) three back-projections of an absorbing disk (from ref. 19).

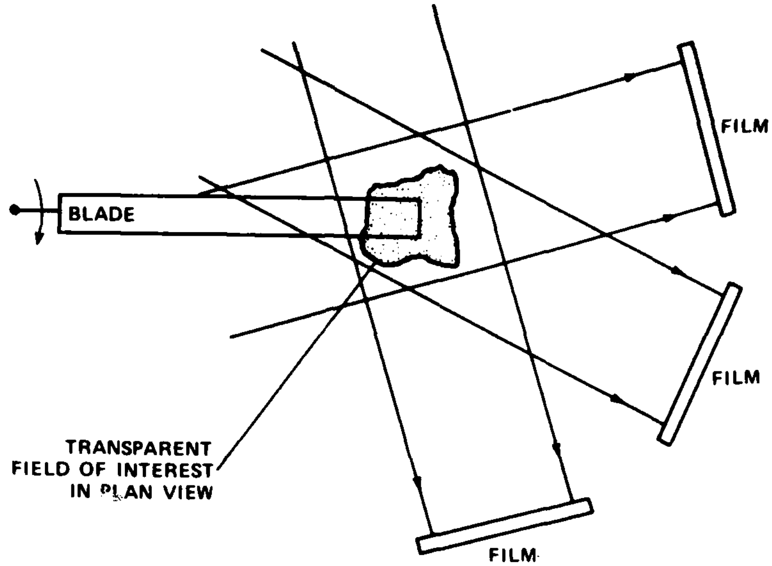

$$\Delta\phi = \int (n - n_0)\, ds = N\lambda$$

Fig. 3 Recording interferograms at various angles around the field of interest for tomographic reconstruction.

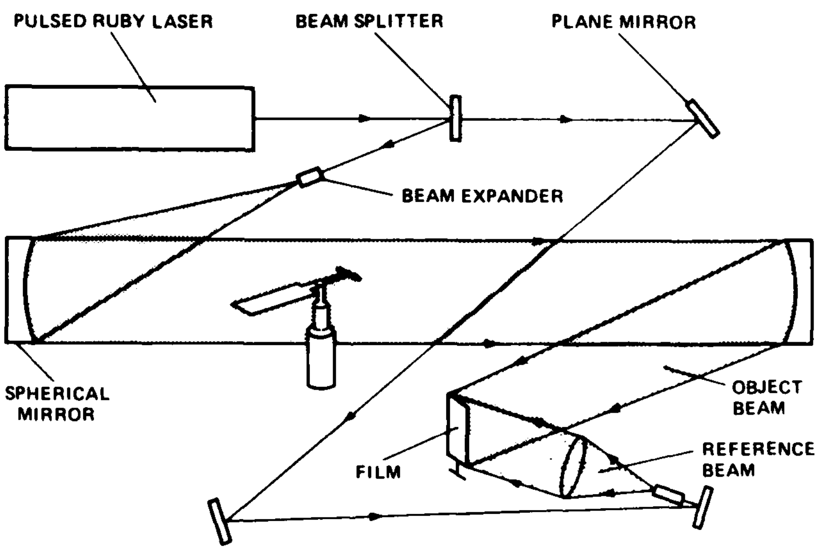

Fig. 4 Schematic drawing of the holographic recording system.

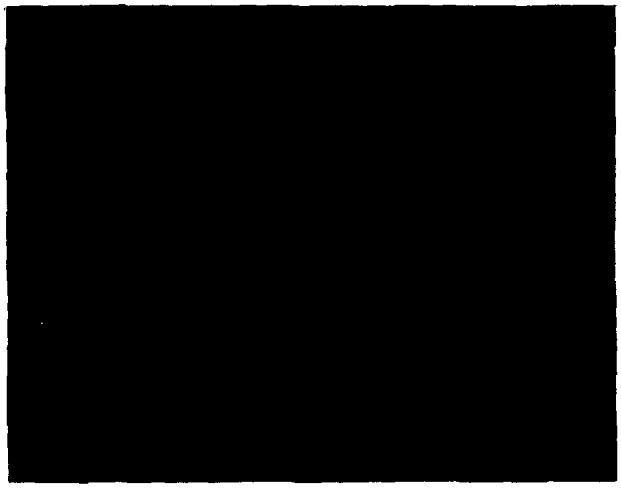

Fig. 5 Holographic setup at Anechoic Hover Chamber.

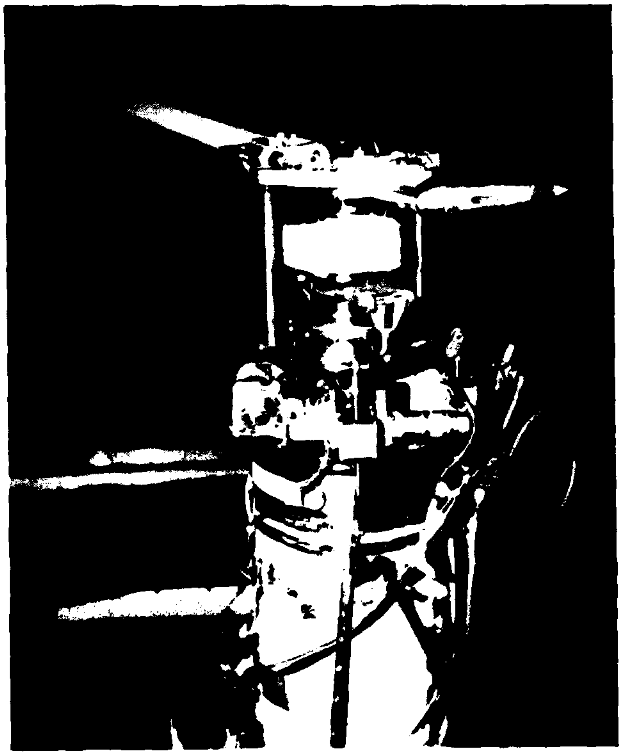

Fig. 6 One-blade rotor with a counterweight balance.

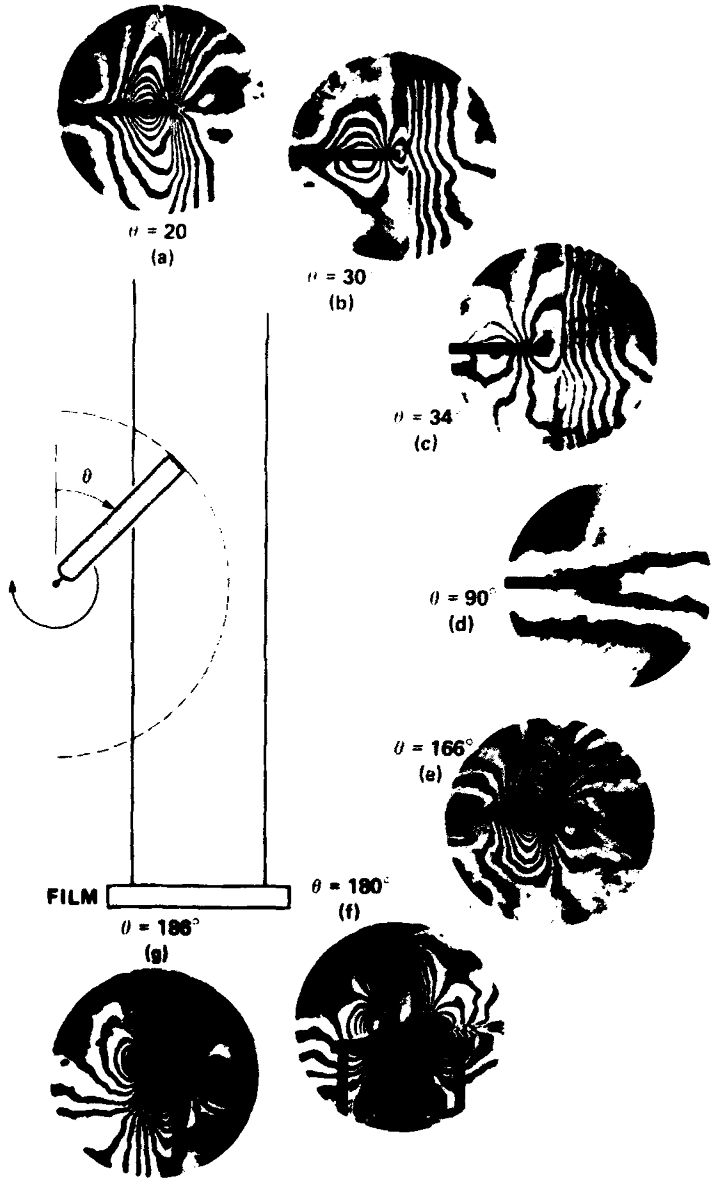

Fig. 7 Top view of the holographic setup and sample interferograms taken at different azimuthal angles.

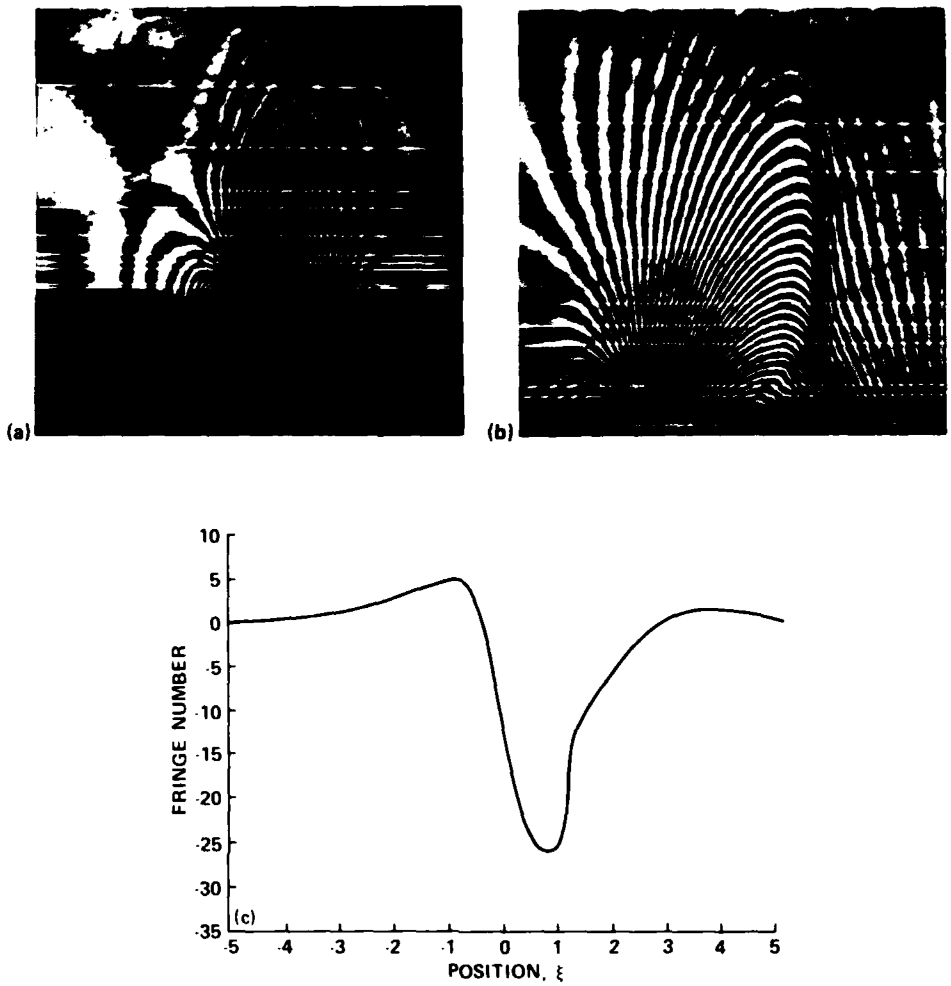

Fig. 8 One-dimensional interferogram evaluation. a) Digitized interferogram with segmented cross section superimposed; b) evaluation of an enlarged section of the interferogram shown in fig. 8a; c) fringe-order function along cross section 3 after combination of several enlarged subsections and rational spline interpolation.

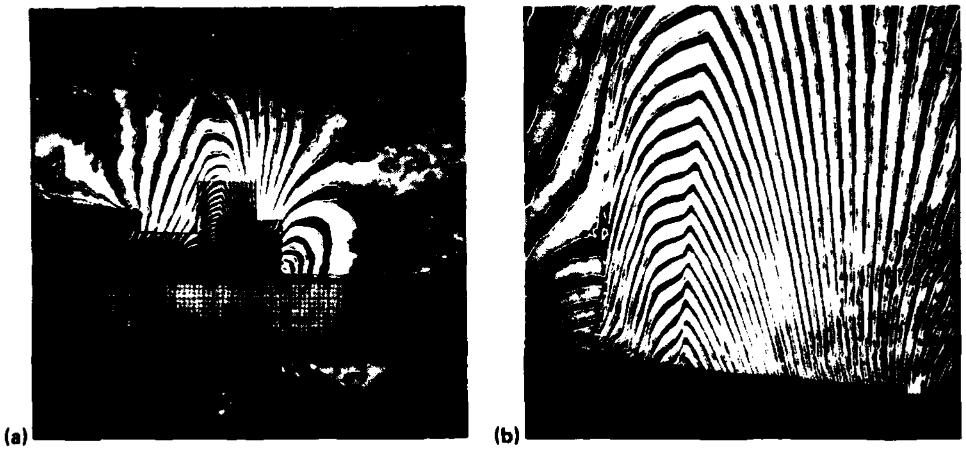

Fig. 9 Example of fringe polygon extraction. a) Original digitized interferogram--extracted fringe polygons are overlayed in white, the border polygon is written in black; b) enlarged digitized part of the same interferogram--extracted fringe polygons are overlayed.

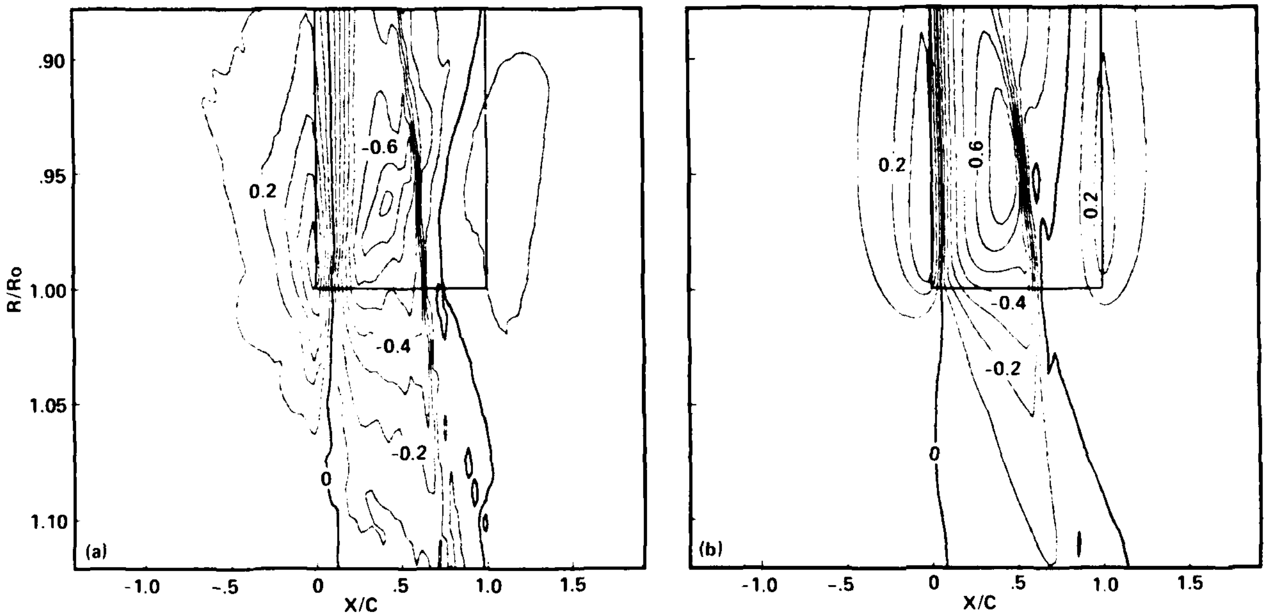

Fig. 10 Pressure-coefficient contours in plan view for Y/C = 0.08 above blade centerline: contour interval = 0.1. a) Holography-CAT reconstruction; b) numerical computation.

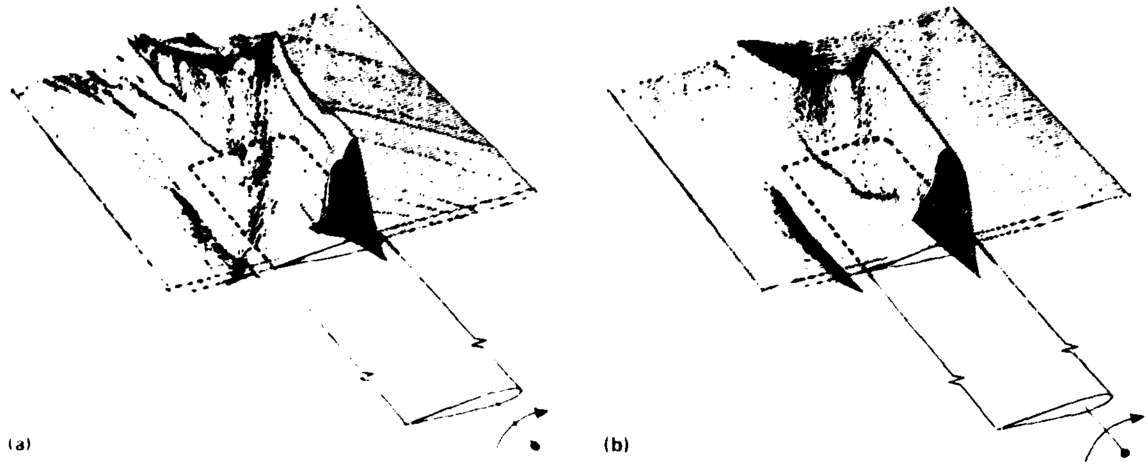

Fig. 11 Pressure-coefficient values for $Y/C = 0.08$ above blade centerline. a) Holography-CAT reconstruction; b) numerical computation.

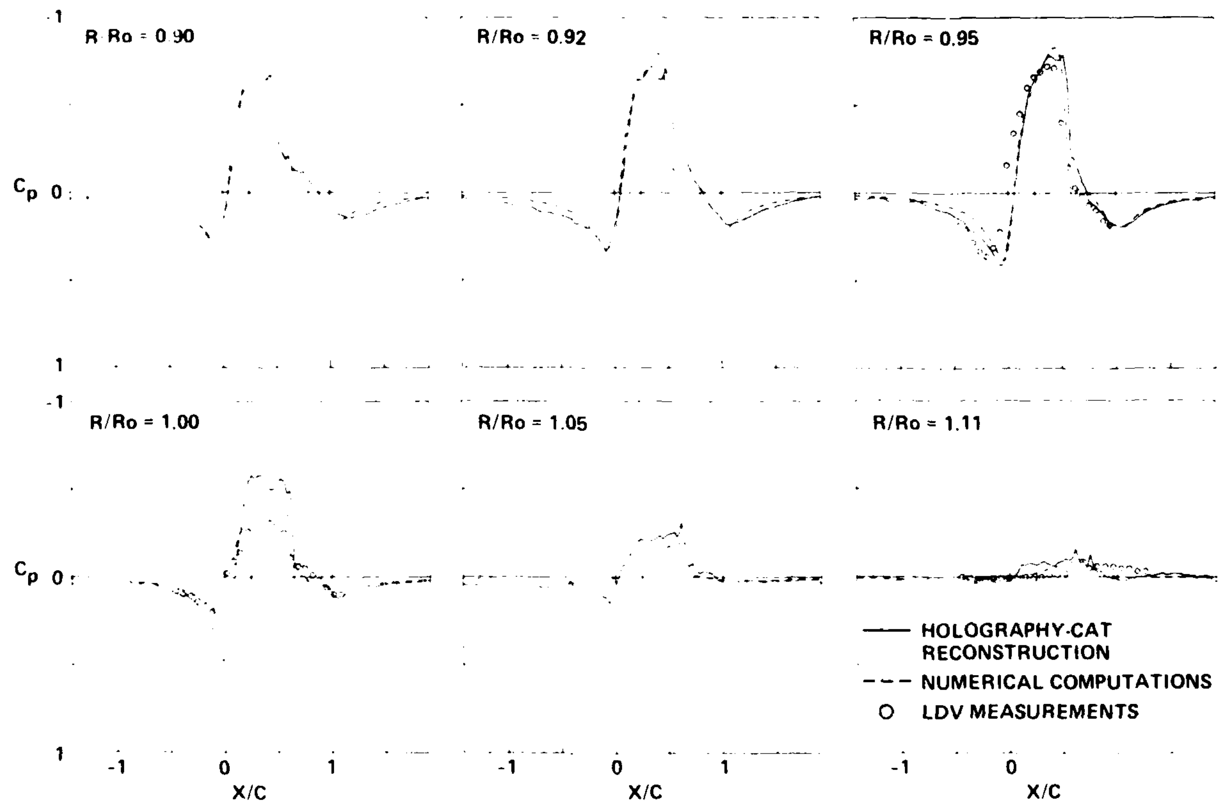

Fig. 12 Pressure-coefficient distributions at six radial locations for $Y/C = 0.08$ above blade centerline. a) $R/R_o = 0.90$; b) $R/R_o = 0.92$; c) $R/R_o = 0.95$; d) $R/R_o = 1.00$; e) $R/R_o = 1.05$; f) $R/R_o = 1.10$.

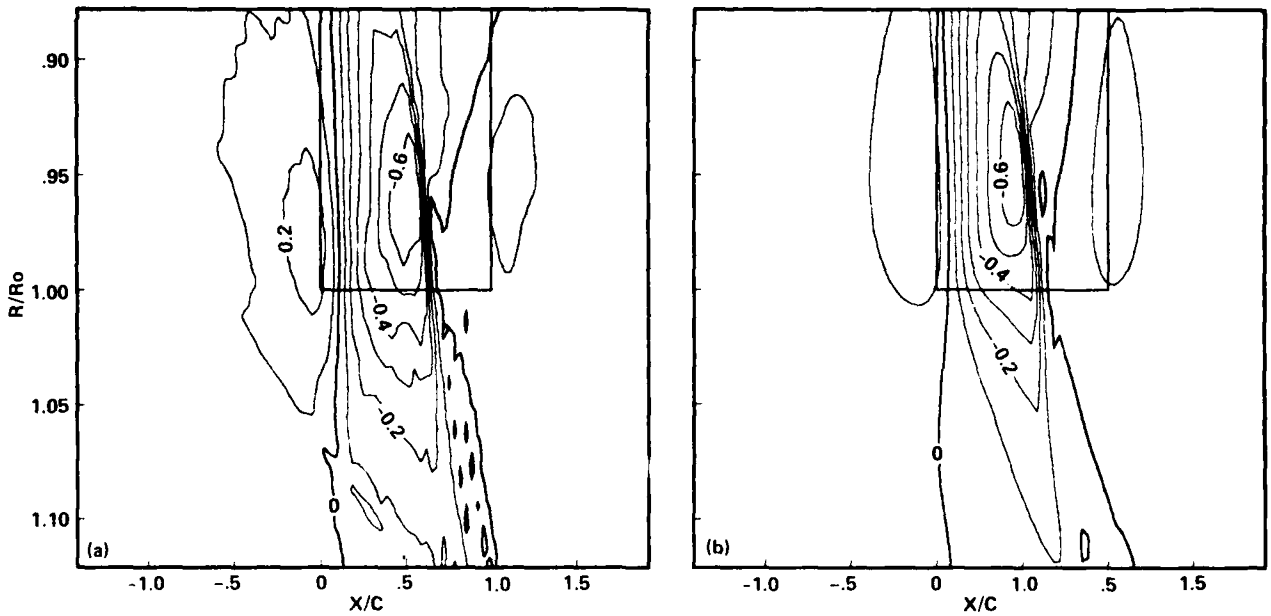

Fig. 13 Pressure-coeficient contours in plan view for Y/C = 0.22 above blade centerline: contour interval = 0.1. a) Holography-CAT reconstruction; b) numerical computation.

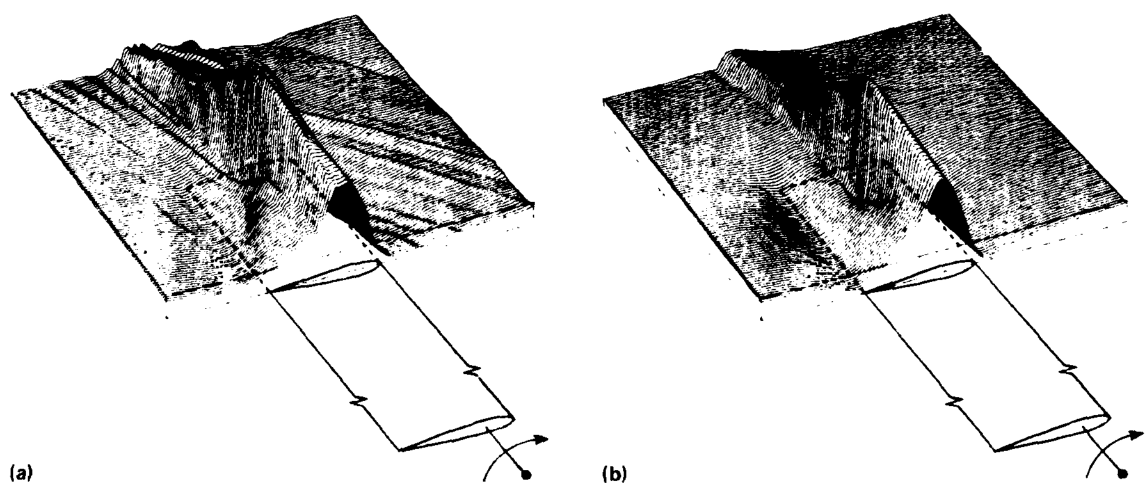

Fig. 14 Pressure-coefficient values for Y/C = 0.22 above blade centerline. a) Holography-CAT reconstruction; b) numerical computation.

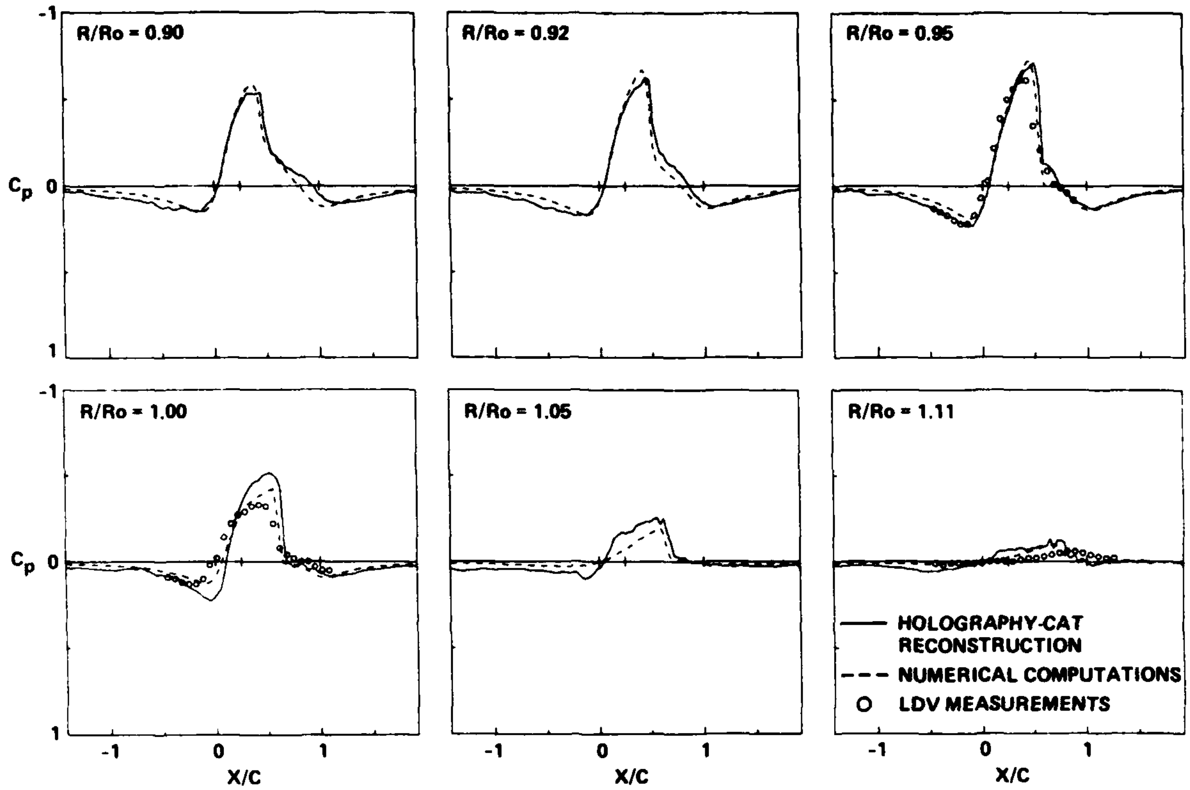

Fig. 15 Pressure-coefficient distributions at six radial locations for $Y/C = 0.22$ above blade centerline. a) $R/R_o = 0.90$; b) $R/R_o = 0.92$; c) $R/R_o = 0.95$; d) $R/R_o = 1.00$; e) $R/R_o = 1.05$; f) $R/R_o = 1.10$.

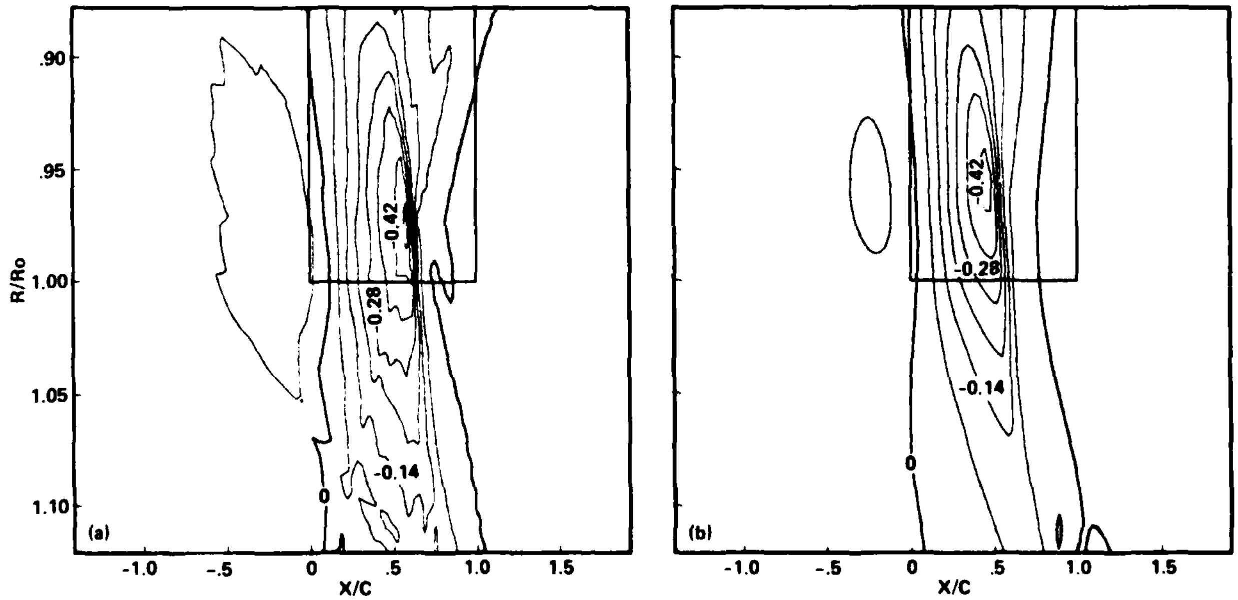

Fig. 16 Pressure-coefficient contours in plan view for $Y/C = 0.49$ above blade centerline: contour interval = 0.07. a) Holography-CAT reconstruction; b) numerical computation.

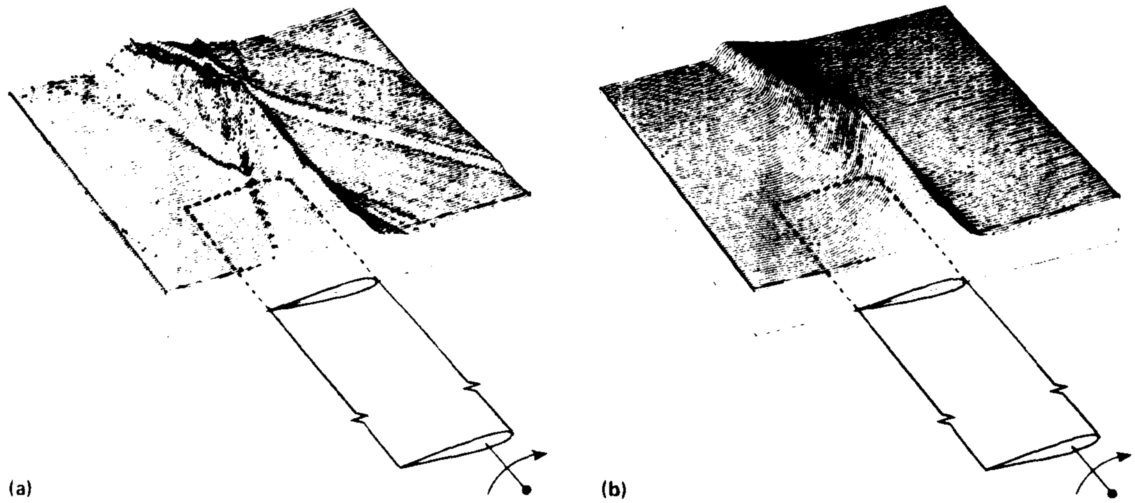

Fig. 17 Pressure-coefficient values for Y/C = 0.49 above blade centerline. a) Holography-CAT reconstruction; b) numerical computation.

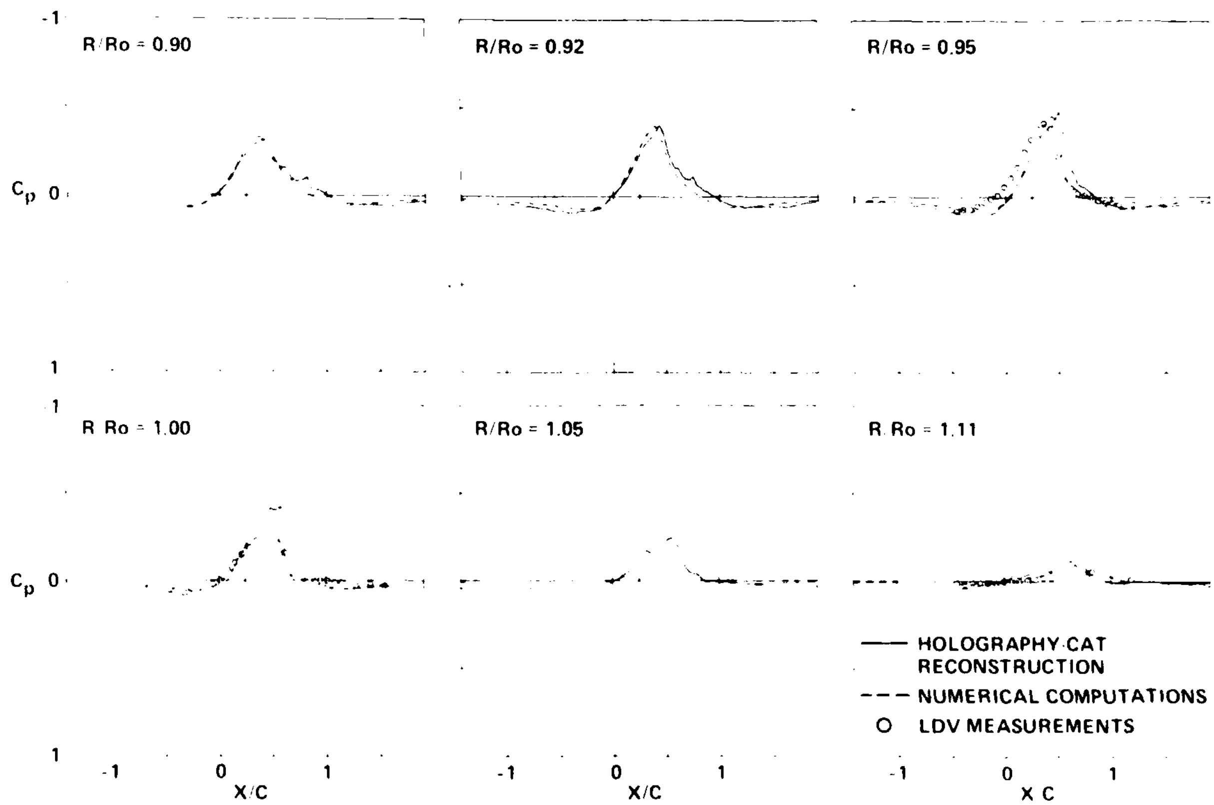

Fig. 18 Pressure-coefficient distributions at six radial locations for Y/C = 0.49 above blade centerline. a) R/R_o = 0.90; b) R/R_o = 0.92; c) R/R_o = 0.95; d) R/R_o = 1.00; e) R/R_o = 1.05; f) R/R_o = 1.10.

1. Report No. NASA TM 86816
USAAVSCOM TR 85-A-10

2. Government Accession No. AD A160 902

3. Recipient's Catalog No.

4. Title and Subtitle
THREE-DIMENSIONAL, TRANSONIC ROTOR FLOW FIELD RECONSTRUCTED FROM HOLOGRAPHIC INTERFEROGRAM DATA

5. Report Date
October 1985

6. Performing Organization Code

7. Author(s)
John K. Kittleson, Yung H. Yu, and Friedhelm Becker*

8. Performing Organization Report No.
85347

9. Performing Organization Name and Address
Ames Research Center and Aeroflightdynamics Directorate, U.S. Army Aviation Research and Technology Activity-AVSCOM, Ames Research Center, Moffett Field, CA 94035

10. Work Unit No.

11. Contract or Grant No.

13. Type of Report and Period Covered

12. Sponsoring Agency Name and Address
National Aeronautics and Space Administration, Washington, DC 20546 and U.S. Army Aviation Systems Command, St. Louis, MO 63120

14. Sponsoring Agency Code
992-21-01

15. Supplementary Notes *Permanent Address: Max-Planck-Institut fuer Stroemungsforschung, Goettingen, West Germany.
Point of Contact: John K. Kittleson, Ames Research Center, MS 215-1, Moffett Field, CA 94035 (415) 694-6062 or FTS 464-6062

16. Abstract

Holographic interferometry and computer-assisted tomography (CAT) are used to determine the transonic flow field of a model rotor blade in hover. A pulsed ruby laser recorded 40 interferograms with a 61 cm-diam view field near the model rotor-blade tip operating at a tip Mach number of 0.90. After digitizing the interferograms and extracting fringe-order functions, the data are transferred to a CAT code. The CAT code then calculates pressure coefficients in several planes above the blade surface. The values from the holography-CAT method compare favorably with previously obtained numerical computations and laser velocimeter measurements at most locations near the blade tip. The results demonstrate the technique's potential for three-dimensional transonic rotor flow studies.

17. Key Words (Suggested by Author(s))
Holographic interferometry
Computer assisted tomography
Helicopter aerodynamics
Transonic aerodynamics

18. Distribution Statement
Unlimited

Subject Category - 35

19. Security Classif. (of this report)	20. Security Classif. (of this page)	21. No. of Pages	22. Price*
Unclassified	Unclassified	21	A02

*For sale by the National Technical Information Service, Springfield, Virginia 22161

END

FILMED

12-85

DTIC